

Gadolinium Complex of DO3A-benzothiazole Aniline (BTA) Conjugate as a Theranostic Agent

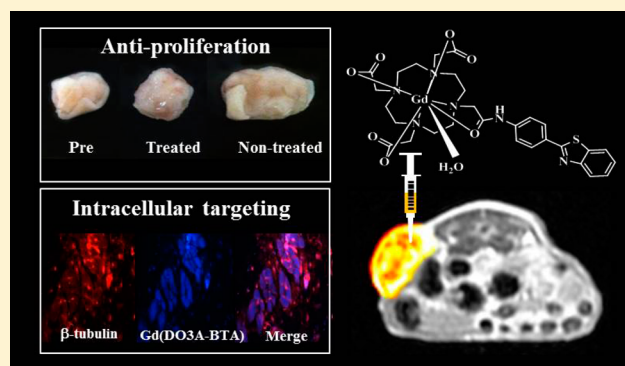
Hee-Kyung Kim,^{†,‡} Min-Kyoung Kang,[†] Ki-Hye Jung,[‡] Sun-Hee Kang,[§] Yeoun-Hee Kim,[#] Jae-Chang Jung,[§] Gang Ho Lee,^{||} Yongmin Chang,^{*,†,‡} and Tae-Jeong Kim^{*,‡}

[†]Department of Medical & Biological Engineering, [‡]Department of Applied Chemistry, [§]Department of Biology, ^{||}Department of Chemistry, [^]Department of Diagnostic Radiology and Molecular Medicine, Kyungpook National University, 80 Daehakro, Bukgu, Daegu, 702-701, Korea

[#]Cheil Eye Hospital, Cheil Eye Research Institute, 803-2 Sinam-1dong, Dong-gu, Daegu, 701-820, Korea

S Supporting Information

ABSTRACT: A gadolinium complex of 1,4,7,10-tetraazacyclododecane-1,4,7-trisacetic acid (DO3A) and benzothiazole-aniline (BTA) of the type [Gd(DO3A-BTA)(H₂O)] has been prepared for use as a single molecule theranostic agent. The kinetic inertness and r_1 relaxivity ($= 3.84 \text{ mM}^{-1} \text{ s}^{-1}$) of the complex compare well with those of structurally analogous Gd-DOTA. The same complex is not only tumor-specific but also intracellular, enhancing MR images of cytosols and nuclei of tumor cells such as MCF-7, MDA-MB-231, and SK-HEP-1. Both DO3A-BTA and Gd(DO3A-BTA) reveal antiproliferative activities as demonstrated by GI₅₀ and TGI values obtainable from the cell counting kit-8 (CCK-8) assays performed on these cell lines. Ex vivo and in vivo monitoring of tumor sizes provide parallel and supportive observations for such antiproliferative activities.



■ INTRODUCTION

Benzothiazoles are fused bicyclic systems possessing diverse biological properties such as anti-inflammatory, antimicrobial, and anticancer effects. As such, a great deal of research activities has been carried out in the past two decades in an effort to develop various benzothiazole derivatives with high antitumor activity.¹ Some representative examples include compounds I shown in Chart 1.²

Even further derivatization of benzothiazole(s) is feasible, and their antitumor properties may be utilized in combination with molecular imaging and therapy. One such endeavor may include the formation of bifunctional chelates (BFCs) incorporating benzothiazole. For instance, the fluorescent rhenium complex conjugated to 2-(4-aminophenyl)-benzothiazole (compounds II, Chart 1) has been reported to enter MCF-7 breast cancer cells. On the basis of these observations, the analogous radioactive complexes ($M = {}^{99m}\text{Tc}$, ${}^{186}\text{Re}$, ${}^{188}\text{Re}$) have been proposed as potential radiopharmaceuticals for single photon emission computed tomography (SPECT) and radioimmunotherapy (RIT).^{3,4} Benzothiazoles labeled with radioisotopes such as ${}^{99m}\text{Tc}$ (compounds III, Chart 1) and ${}^{11}\text{C}$ have been proposed as potential probes for β -amyloid plaques in the brain.^{5,6} More recently, conjugates of benzothiazoles with 1,4,7,10-tetraazacyclododecane-1,4,7-tris-tert-butyl acetate (DO3A) (compounds IV, Chart 1) have been

employed as multimodal imaging probes such as magnetic resonance imaging (MRI)/optical and MRI/SPECT.^{7,8}

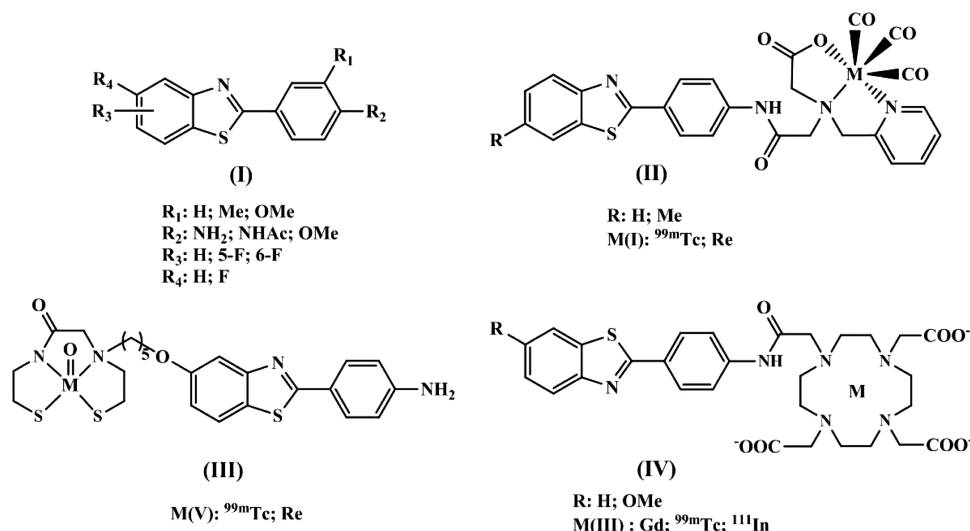
Despite such widespread use of benzothiazole-based BFCs, their uses have been limited solely to molecular imaging in vitro, not to mention their application as therapeutic agent in vivo. It is thus to be highly motivated to investigate the possibility of expanding the scope of benzothiazole-based BFCs to the area of theranostics (a coinage of diagnostic and therapy). This notion can be justified as we observe the recent thrust to put together imaging and therapeutic functions in a single molecule.

In particular, our motivation comes from the observations that the complexes of DO3A-benzothiazole conjugate (IV) serve as multimodal MRI/optical probes. Thus, we would like to pursue further the therapeutic propensity of the closely related Gd complex of the type [Gd(DO3A-benzothiazole aniline)(H₂O)] (1) in the hope that it may serve as a single molecule theranostic agent. In this connection, it has to be noted that although numerous types of gadolinium nanoparticles (GdNPs) with multiple functionalities have been developed,⁹ most of which carry either multimodal,¹⁰ therapeutic,¹¹ or theranostic functionality,¹² their application

Received: August 6, 2013

Published: September 24, 2013

Chart 1. Various Benzothiazoles Used in Imaging and Therapy



in nanomedicine is still in its infancy due to the toxicological problems inherently connected with slow excretion rates.¹³

In contrast, however, small molecule Gd-chelates would provide a promising substitute to eliminate or overcome the problems inherent to GdNPs-based pharmaceuticals. Gd-motexafin is a novel example for an antineoplastic drug capable of disrupting cancer cell antioxidant systems, thus contributing to cellular death. This same complex has demonstrated an additional functionality of radiosensitizing the cancer.¹⁴ A more recent example includes a heterobimetallic Gd–Pt complex incorporating DTPA and terpyridine (terpy) as chelate. This complex is known to intercalate DNA due to the presence of the Pt(terpy) moiety, an analogue of cisplatin. The author has proposed that the Gd/Pt complex might have potentiality in gadolinium neutron-capture (GdNCT).¹⁵ The use of Gd complexes (including GdNPs) in GdNCT has become the topic of recent interest,^{16,17} as they are closely related to the well-established boron neutron-capture therapy (BNCT).^{18,19} We now wish to report the design and synthesis of Gd(DO3A-BTA) for use as a theranostic agent. To the best of our knowledge, we believe this complex to be a rare example of small molecule Gd-chelate based theranostic agent.

EXPERIMENTAL SECTION

General Remarks. All reactions were carried out under an atmosphere of dinitrogen using the standard Schlenk techniques. Solvents were purified and dried using standard procedures. *N*-(4-(Benzo[*d*]thiazol-2-yl)phenyl)-2-chloroacetamide⁴ and DO3A(^{*t*}Bu)₃ (= 1,4,7,10-tetraazacyclododecane-1,4,7-tris-*tert*-butyl acetate)²⁵ were prepared according to the literature methods. All other commercial reagents were purchased from Aldrich and used as received unless otherwise stated. Deionized water was used for all experiments. The ¹H NMR experiment was performed on a Bruker Avance 400 spectrometer by the Center for Instrumental Analysis, Kyungpook National University (KNU). Chemical shifts were given as *d* values with reference to TMS as an internal standard. Coupling constants are in Hz. Elemental analyses were performed by Center for Instrumental Analysis, KNU in Daegu. FAB-mass spectra were obtained by using a JMS-700 model (Jeol, Japan) mass spectrophotometer by Korea Basic Science Institute (KBSI). The HPLC system (high pressure liquid chromatography, KNAUER, Berlin, Germany) equipped with a Develosil ODS-HG-5 column (6.0 mm × 250 mm; Nomura Chemical Co., Ltd., Aichi, Japan) was used for the measurement. Elution conditions were as follows: a mixture of an aqueous solution of TFA

(0.1%, v/v) and an acetonitrile solution of TFA (0.1%, v/v) with a 30 min isocratic elution (95 vs 5%) at a flow rate of 1.4 mL/min was used. The purity of all products was determined with purity above 95% by elemental analysis. The purity of DO3A-BTA and Gd(DO3A-BTA) was double-checked by analytical and semipreparative reversed-phase HPLC with a UV-vis detection probing at 240 nm (Supporting Information Figure S5).

Synthesis and Characterization. *tert*-Butyl 2,2',2''-(10-(2-(4-(Benzo[*d*]thiazol-2-yl)phenylamino)-2-oxoethyl)-1,4,7,10-tetraazacyclododecane-1,4,7-triyl)triacetate. To a mixture of DO3A(^{*t*}Bu)₃ (1.1 g, 2.2 mmol) and NaHCO₃ (0.5 g, 6.6 mmol) in DMF (10 mL) was added dropwise a solution of *N*-(4-(benzo[*d*]thiazol-2-yl)phenyl)-2-chloroacetamide (1.0 g, 3.3 mmol) in DMF (10 mL). After stirring for 18 h at RT, water (200 mL) was added dropwise and the mixture was stirred for 2 h at RT. The precipitate was filtered and washed with water. The crude product thus obtained was further purified by column chromatography (silica, CH₂Cl₂/MeOH, 97:3) to give a white solid. Yield: 0.5 g (30%). ¹H NMR (CDCl₃): δ = 8.09–8.07 (*d*, 2H, phenyl), 8.02–8.00 (*d*, 1H, benzothiazole), 7.92–7.90 (*d*, 2H, phenyl), 7.86–7.85 (*d*, 1H, benzothiazole), 7.47–7.43 (*t_b*, 1H, benzothiazole), 7.36–7.32 (*t_b*, 1H, benzothiazole), 3.05–2.85 (*m*, 8H, –CH₂CO₂, –CH₂CONH), 2.61–2.02 (*m*, 16H, CH₂ in the cyclen ring). Anal. Calcd for C₄₁H₆₄N₆O₇S·4HCl: C, 53.13; H, 6.96; N, 9.07; S, 3.46. Found: C, 52.93; H, 6.62; N, 8.97; S, 3.17. HR-FABMS (*m/z*): calcd for C₄₁H₆₀N₆O₇SNa, 803.4142 ([MNa]⁺); found, 803.4142 ([MNa]⁺).

DO3A-BTA. Deprotection of *tert*-butyl was performed as follows: *tert*-Butyl 2,2',2''-(10-(2-(4-(benzo[*d*]thiazol-2-yl)phenylamino)-2-oxoethyl)-1,4,7,10-tetraazacyclododecane-1,4,7-triyl)triacetate (1.0 g, 1.3 mmol) dissolved in a mixture of TFA/CH₂Cl₂ (1:1, 20 mL) was stirred at RT for 24 h, after which the solution was evaporated under a reduced pressure. The crude product was dissolved in MeOH (10 mL) and precipitated with diethyl ether (100 mL) to yield a yellowish white solid. Yield: 0.6 g (68%). ¹H NMR (methanol-*d*₄): δ = 8.00–7.95 (*m*, 4H, phenyl), 7.79–7.77 (*m*, 2H, benzothiazole), 7.53–7.50 (*t*, 1H, benzothiazole), 7.43–7.40 (*t*, 1H, benzothiazole), 3.86–3.61 (*m*, 8H, –CH₂CO₂, –CH₂=CO), 3.50–3.14 (*m*, 16H, CH₂ in the cyclen ring). Anal. Calcd for C₂₉H₄₆N₆O₁₂S·5H₂O: C, 49.56; H, 6.60; N, 11.96; S, 4.56. Found: C, 49.57; H, 6.20; N, 12.33; S, 4.45. HR-FABMS (*m/z*): calcd for C₂₉H₃₆N₆O₇SNa, 635.2264 ([MNa]⁺); found, 635.2264 ([MNa]⁺). HPLC (analytical, 2.1 mm × 250 mm; flow rate, 1.4 min/L; retention time, 24.65 min).

Gd(DO3A-BTA). DO3A-BTA (0.5 g, 0.8 mmol) was dissolved in water (15 mL) to which was added gadolinium(III) chloride hexahydrate (0.3 g, 0.8 mmol). The mixture was stirred at RT for 18 h, during which time pH of the solution was periodically adjusted to 7.0–7.5 with NaOH (1.0 M). Water was removed by evaporation,

and the remaining oily product was taken up in a minimum amount of water (~5 mL) to be added dropwise to acetone for precipitation. The white precipitate thus formed was removed by filtration, washed with acetone, and dried under vacuum. The precipitate (~0.6 g) was redissolved in a minimum amount of water to elute in Amberlite XAD 16N (25 g). Any inorganic salts such as NaCl and the Gd^{3+} ion were removed initially by eluting with water and the product by MeOH (25 mL). The yellowish white solid left after removal of MeOH was washed several times with acetone and dried under vacuum to yield an off-white, hygroscopic solid (0.5 g, 82%). The absence of the free Gd^{3+} ion was further confirmed by the xylenol orange test, and the purity (above 95%) determined by HPLC (analytical, 2.1 mm \times 250 mm; flow rate, 1.4 mL/min; retention time, 21.87 min). Anal. Calcd for $C_{29}H_{59}GdN_6O_{20}S \cdot 13H_2O$: C, 34.79; H, 5.94; N, 8.39; S, 3.26. Found: C, 34.87; H, 4.09; N, 8.63; S, 2.93. HR-FABMS (m/z): calcd for $C_{29}H_{34}GdN_6O_7S$, 768.1445 ($[MH]^+$); found, 768.1456 ($[MH]^+$).

Transmetalation Kinetics and Determination of Kinetic Constants. This experiment was performed according to the literature method.²⁰ It is based on the evolution of the water proton relaxation rate (R_1^p) of a buffered solution (phosphate buffer, pH 7.4) containing 2.5 mmol/L gadolinium complex and 2.5 mmol/L $ZnCl_2$. Then 10 μ L of a 250 mmol/L solution of $ZnCl_2$ is added to 1 mL of a buffered solution of the paramagnetic complex. The mixture is vigorously stirred, and 300 μ L is taken up for the relaxometric study. A control study, run on Gd-DO3A-BT (Gadovist), Gd-EOB-DTPA (Primovist), Gd-BOPTA (Multihance), Gd-DTPA-BMA (Omniscan), and Gd-DOTA (Dotarem) with zinc acetate, has given results identical to those obtained in the presence of $ZnCl_2$. The R_1^p relaxation rate is obtained after subtraction of the diamagnetic contribution of the proton water relaxation from the observed relaxation rate $R_1 = (1/T_1)$. The measurements were performed on a 3 T whole body system (Magnetom Tim Trio, Siemens, Germany) at room temperature.

Relaxivity. T_1 measurements were carried out using an inversion recovery method with a variable inversion time (TI) at 1.5 T (64 MHz). The magnetic resonance (MR) images were acquired at 35 different TI values ranging from 50 to 1750 ms. T_1 relaxation times were obtained from the nonlinear least-squares fit of the signal intensity measured at each TI value. For T_2 measurements, the CPMG (Carr–Purcell–Meiboom–Gill) pulse sequence was adapted for multiple spin–echo measurements. Then 34 images were acquired with 34 different echo time (TE) values ranging from 10 to 1900 ms. T_2 relaxation times were obtained from the nonlinear least-squares fit of the mean pixel values for the multiple spin–echo measurements at each echo time. Relaxivities (R_1 and R_2) were then calculated as an inverse of relaxation time per mM. The determined relaxation times (T_1 and T_2) and relaxivities (R_1 and R_2) are finally image-processed to give the relaxation time map and relaxivity map, respectively.

MR Imaging and Image Analysis. In vitro MR images were taken with a 1.5 T (T) MR unit (GE Healthcare, Milwaukee, WI, USA) equipped with a surface coil. The imaging parameters for SE (Spin Echo) are as follows: repetition time (TR) = 300 ms; echo time (TE) = 12 ms; 15 mm field of view (FOV); 256 \times 256 matrix size; 1.2 mm slice thickness; number of acquisition (NEX) = 20.

All animal experiments were performed in accordance with the rules of the animal research committee of Kyungpook National University. Seven-week normal female balb/c nude mice with weights of 18–25 g were used for the MRI. Fifteen-week-old female balb/c nude mice bearing MCF-7 tumor were used for the MRI. The mice were anesthetized by 1.5% isoflurane in oxygen. Measurements were made before and after injection of Gd(DO3A-BTA) and Gd-DOTA (Dotarem) via tail vein. The amount of CA per each injection is 0.1 mmol [Gd]/kg for MR images. After each measurement, the mouse was revived from anesthesia and placed in the cage with free access to food and water. During these measurements, the animals were maintained at approximately 37 °C using a warm water blanket. MR images were taken with a 1.5 T (T) MR unit (GE Healthcare, Milwaukee, WI, USA) equipped with a homemade small animal RF coil. The coil was of the receiver type with its inner diameter being 50 mm. The imaging parameters for spin–echo (SE) are as follows: repetition time (TR) = 300 ms; echo time (TE) = 13 ms; 8 mm field

of view (FOV); 192 \times 128 matrix size; 1.2 mm slice thickness; number of acquisition (NEX) = 8. Images were obtained for 240 min after injection. The anatomical locations with enhanced contrast were identified with respect to heart, kidney, and liver on postcontrast MR images. For quantitative measurement, signal intensities in specific regions of interest (ROI) measured using Advantage Window software (GE Medical, USA). The contrast-to-noise ratio (CNR) was calculated using eq 1, where SNR is the signal-to-noise ratio.

$$CNR = (SNR_{post} - SNR_{pre}) \quad (1)$$

In Vivo Therapy. The subcutaneous tumor model was established in a nude mouse as described in tumor model session in order to investigate the therapeutic effect of Gd(DO3A-BTA) in vivo. When the average volume of MDA-MB-231 reached 50 mm³ six to seven weeks after implantation of cells, two groups of mice with each bearing five of those were assigned, respectively, to the tests for control and Gd(DO3A-BTA). The volume of the solution in each test was 70 μ L (0.1 mmol/kg, 35–50 mM stock solution) and injected once a day for 3 weeks. Tumor sizes were measured at given time points either with a caliper or with MR images. Tumor size measured by caliper is given as V/V_0 (V_0 = the initial volume), while that measured by MRI is calculated using eq 2.

$$\begin{aligned} \text{tumor size} &= \text{number of pixels of tumor} \times \text{pixel area} \\ &\times \text{slice thickness} \end{aligned} \quad (2)$$

Biodistribution. Gd(DO3A-BTA) was administered intravenously as a bolus (0.1 mmol/kg) in a tail vein of nine female mice bearing MDA-MB-231 tumor (balb/c nude mice; 18–25 g). The mice were anesthetized and killed by means of exsanguinations from the vena cava at each time point (after 1, 6, and 24 h injection time). The gadolinium concentration was measured in tissues (liver, spleen, gall bladder, bladder, kidneys, lung, tumor, blood, heart, brain, and intestine). The gadolinium concentration was determined by digesting the tissues with HNO_3 (65%) at 180 °C for 120 min and measuring the concentration in the clear diluted solution by inductively coupled plasma atomic emission spectrometry (ICP-AES, Optima 7300DV, PerkinElmer, USA). Detection limit of this method is 0.01 ppm.²⁶

Cell Culture. The culture medium consisted of Dulbecco's Modified Eagle's Medium (DMEM; Gibco Invitrogen, Carlsbad, CA) or Roswell Park Memorial Institute (RPMI, Gibco Invitrogen, Carlsbad, CA), 10% (v/v) fetal bovine serum (FBS), and 1% (v/v) penicillin–streptomycin. Cells were plated at a density of 2×10^5 cells/35 mm dish, incubated during overnight for stabilization and then treated with Gd for 24 h in serum depletion media.

Tumor Model. The MCF-7 and MDA-MB-231 tumor cells (10^6 cell mL⁻¹) suspended in DMEM or RPMI-1640 medium without fetal bovine serum and penicillin–streptomycin were inoculated into subcutaneous tissue (sc) of female BALB/c nude mice (7 weeks, 18–25 g of body weight). The nude mice were anesthetized (1.5% isoflurane in oxygen). The MR experiments were carried out 6 or 7 weeks after tumor cell implantation.²⁷

Cell Fractions for MRI. MCF-7, MDA-MB-231, and SK-HEP-1 cells were plated 2×10^5 in 35 mm dishes. The DMEM or RPMI growth medium was removed, and then Gd(DO3A-BTA) (100 μ M) in DMEM or RPMI serum depletion media for 24 h. The cells were washed with phosphate buffered saline (PBS) and harvested. For cell fractionation, cancer cells were lysed by three cycles of freezing and thawing in PBS, and lysates centrifuged at 1000 rpm for 5 min at 4 °C. The supernatant was cytosolic fraction, and the first pellet was resuspended in radioimmunoprecipitation assay (RIPA) buffer for 1 h at 4 °C and centrifuged at 12,000 rpm for 10 min at 4 °C. The supernatant corresponded to RIPA buffer-soluble membrane fraction and the final pellet contained nuclei and cell organelles. Collected cells were performed MR imaging by using a 1.5T MRI scanner.

Cell Viability Assay (in Vitro Growth Inhibition). MCF-7, MDA-MB-231, and SK-HEP-1 cells were plated 1×10^4 in 96-well plate. The DMEM or RPMI growth medium was removed, and then Gd(DOTA-BTA) in DMEM or RPMI serum depletion media for 24 h. Then the live cell count was assayed using CCK-8 (Dojindo,

Sunnyvale, CA) according to the manufacturer's protocol. In brief, 10 μL of CCK-8 solution was added to each well, and the samples were incubated for 4 h before the absorbance was measured at 450 nm.

Fluorescence and UV Microscope Images of Cells. Gd-(DOTA-BTA) injected tissue was harvested and fixed with 4% paraformaldehyde (PFA). The tissue was then dehydrated through an ethanol series, cleared by soaking in xylene, embedded in paraffin, and sectioned (5 mm) using a microtome RM 2125RT (Leica, Wetzlar, Germany). The specimen was incubated overnight with monoclonal antibodies against β -tubulin. Images were captured using a Zeiss fluorescence microscope (TRITC-546 nm, UV-385 nm).

FACS Analysis. Cells ($\sim 1 \times 10^6$) were suspended in 100 μL of PBS, and 200 μL of 95% ethanol were added while vortexing. Then the cells were incubated at 4 $^{\circ}\text{C}$ for 1 h, washed with PBS, and resuspended in 250 μL of 1.12% sodium citrate buffer (pH 8.4) together with 12.5 μg of RNase. Incubation was continued at 37 $^{\circ}\text{C}$ for 30 min. The cellular DNA was then stained by applying 250 μL of propidium iodide (PI) (50 $\mu\text{g}/\text{mL}$) for 30 min at room temperature. The PI stained cells were analyzed by fluorescent activated cell sorting (FACS) on a FACScan flow cytometer to determine relative DNA content based on red fluorescence.

Cell Morphology. Primary cultured normal conjunctival cell (passage 4–5) and cancer cells were plated 2×10^5 in 35 mm dishes. Cells were exposed with Gd(DOTA-BTA) for 24 h with serum depletion media. The morphological features of cultured cells were observed by phase-contrast microscopy.

RESULTS AND DISCUSSION

Synthesis. The bifunctional chelate and its Gd(III) complex, each abbreviated as DO3A-BTA and Gd(DO3A-

BTA), were prepared according to the literature method with a slight modification (Supporting Information Scheme S1). DO3A-BTA can be readily prepared by acid hydrolysis with TFA of the corresponding *tert*-butyl ester which is in turn prepared from simple conjugation of DO3A(^tBu)₃ with benzothiazole–chloroacetylaniline. The reaction of DO3A-BTA with GdCl₃ resulted in the formation of the corresponding Gd(III) complex of the type [Gd(DO3A-BTA)(H₂O)]₃ as a hygroscopic white solid.

The formation of both DO3A-BTA and its Gd-complex was confirmed by microanalysis and spectroscopic techniques such as ¹H NMR, HRFAB- and MALDI-TOF mass spectrometry. The Gd(III) complex was identified as a hydrate of 13 water molecules [Gd(DO3A-BTA)(H₂O)]₃·13H₂O as confirmed by microanalytical results.

Kinetic Inertness. The kinetic inertness for Gd(DO3A-BTA) is typically represented by the evolution of the normalized paramagnetic longitudinal relaxation rates, $R_1^P(t)/R_1^P(0)$ as a function of time along with those for Gd-DOTA, Gd-BOPTA, Gd-EOB-DTPA, Gd-DO3A-BT, and Gd-DTPA-BMA for comparative purposes (Supporting Information Figure S1). Here, the relative value of R_1^P at any time t is a good estimator of the extent of transmetalation of gadolinium by zinc. Of various endogenous ions, Zn²⁺ has been noted to displace more gadolinium ions due to its higher concentration in the blood than any other ions such as Cu(II), Ca(II), and K(I).²⁰ As might be expected, our new Gd complex exhibits high kinetic stability comparable with those of Gd-DO3A-BT and Gd-DOTA employing the same type of macrocyclic chelate. Virtually no significant changes in relaxivity is observed either with DOTA or DO3A for as long as 3 days. In contrast, however, other MRI contrast agents (CAs) employing the acyclic DTPA analogues show significant drops in R_1 for the same period of time.

Relaxivity. Gd(DO3A-BTA) reveals relaxivities in PBS comparable well with those of Gd-DOTA (Table 1). The

Table 1. Relaxivity Data of Gd-DOTA and Gd(DO3A-BTA) in PBS (64 MHz, 293K)

	r_1 (mM ⁻¹ s ⁻¹)	r_2 (mM ⁻¹ s ⁻¹)
Gd(DO3A-BTA)	3.84 ± 0.19	4.07 ± 0.19
Gd-DOTA	3.69 ± 0.12	3.98 ± 0.19

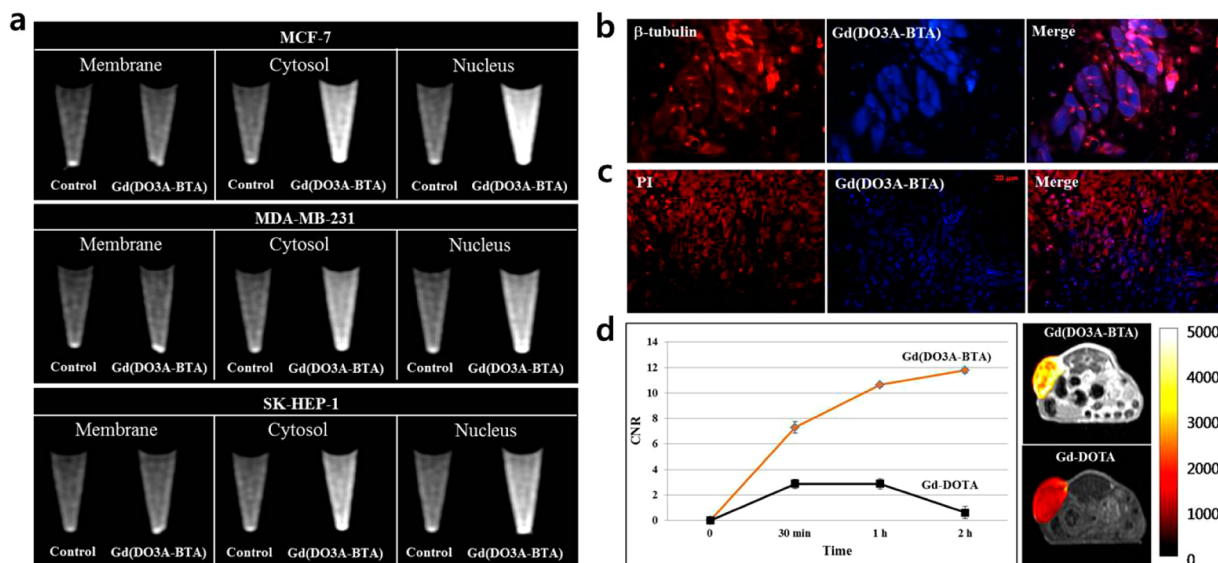


Figure 1. (a) T_1 -weighted MR images of MCF-7, MDA-MB-231, and SK-HEP-1 cell fractions incubated with Gd(DO3A-BTA). (b) UV–vis images of MCF-7 tumor tissue of mice ($\times 400$): tissue stained with β -tubulin (left), tissue obtained by tail vein injection with Gd(DO3A-BTA) (middle), and merged image of two (right). (c) UV–vis images of MDA-MB-231 tumor tissue ($\times 100$): tissue stained with PI (left), tissue obtained by tail vein injection with Gd(DO3A-BTA) (middle), and merged image of two (right). (d) CNR profiles and in vivo MR axial images of mice bearing MDA-MB-231 tumor obtained with Gd(DO3A-BTA) and Gd-DOTA, measured 1 h after injection.

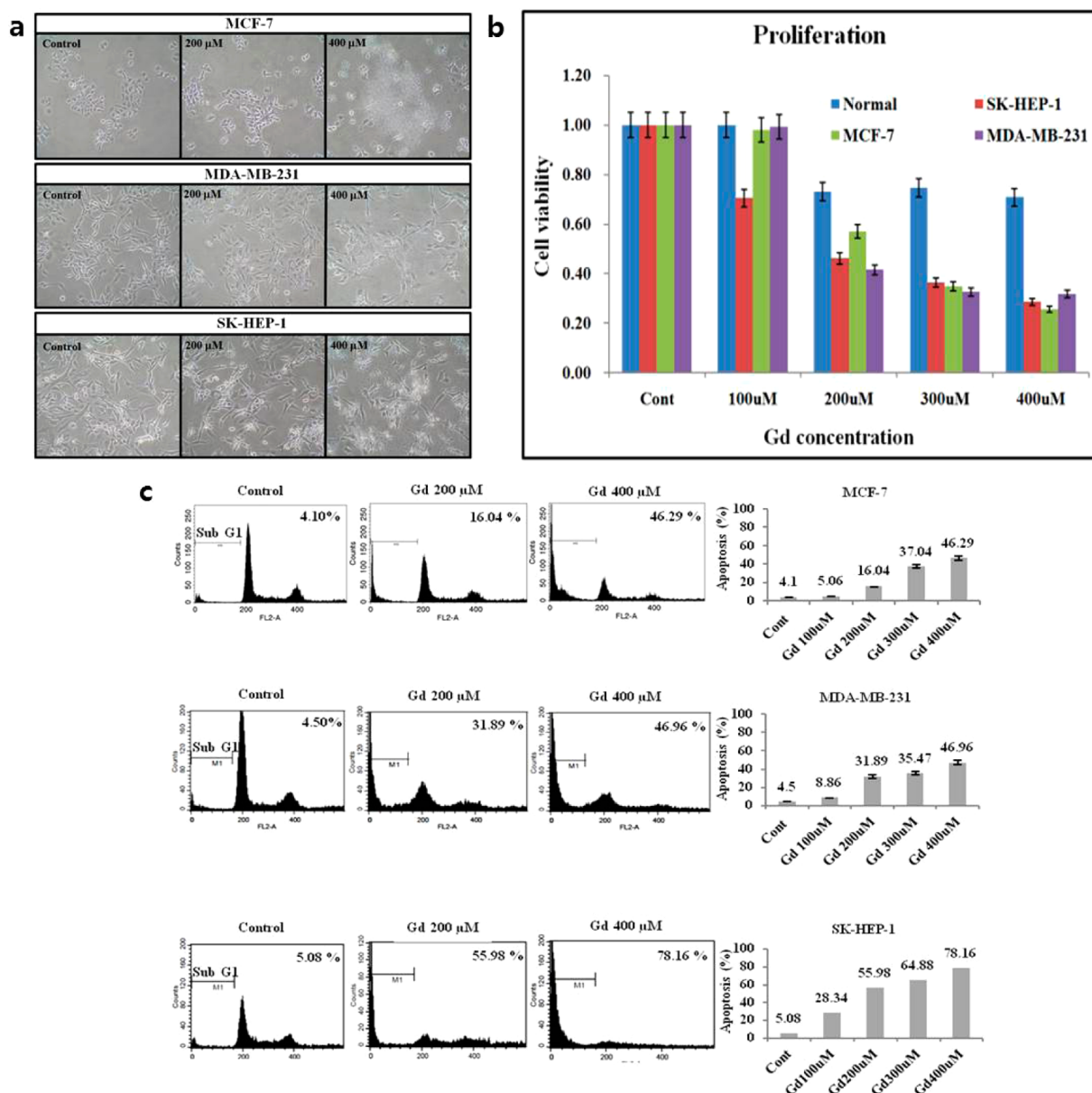


Figure 2. (a) phase-contrast microscopic images of morphological changes in cultured MCF-7, MDA-MB-231, and SK-HEP-1 cells with Gd(DO3A-BTA). (b) Proliferation of normal conjunctival cell, MCF-7, MDA-MB-231, and SK-HEP-1 after treatment with various concentrations of Gd(DO3A-BTA). (c) Flow cytometric (left) and quantitative analysis of apoptosis for MCF-7, MDA-MB-231, and SK-HEP-1 cells after treatment with Gd(DO3A-BTA). Apoptosis was analyzed as a sub-G1 fraction by FACS.

Table 2. In Vitro Activities of DO3A-BTA and Gd(DO3A-BTA) in Cancer Cell Lines

	MCF-7	MDA-MB-231	SK-HEP-1
DO3A-BTA			
GI ₅₀ [μM]	715.57	669.57	625.33
TGI [μM]	1923.28	1637.75	1656.83
Gd(DO3A-BTA)			
GI ₅₀ [μM]	258.48	237.47	203.43
TGI [μM]	555.89	637.82	706.73

presence of the lipophilic BTA moiety in DO3A-BTA seems to exert little effect on the thermodynamic stability of Gd(DO3A-BTA) in PBS. In comparison, its presence seems to be a little more significant in HSA because of the lipophilic interaction with HSA. This point will be discussed in the next section.

Interaction with HSA. Proton longitudinal paramagnetic relaxation rate of Gd(DO3A-BTA) (Supporting Information Figure S2) and the corresponding binding constant K_a (Supporting Information Table S1) provide the evidence for the noncovalent lipophilic interaction between the chelate DO3A-BTA. One may expect a higher K_a value with DO3A-BTA than with other DOTA derivatives devoid of any aromatic moieties. We have found K_a for Gd(DO3A-BTA) to be greater almost by an order of one than those for Gd-DOTA and Gd-EOB-DTPA (Supporting Information Table S1). Gd-DOTA is a well-known extracellular fluid (ECF) agent incorporating DOTA as a chelate, and one may expect little of such interaction. Gd-EOB-DTPA, a liver-specific MRI CA, also exhibits unexpectedly low interaction in spite of the presence of aromatic moiety in the DTPA ligand.^{21,22}

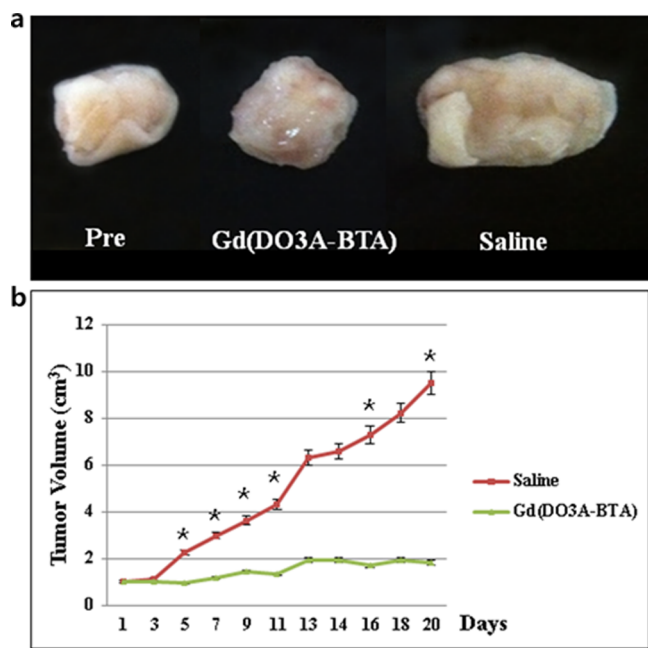


Figure 3. (a) Ex vivo images of MDA-MB-231 tumors derived from balb/c nude mice treated with Gd(DO3A-BTA) and saline after the end of treatment. (b) Changes in tumor volumes (*t* test, $p < 0.05$) as measured by a caliper.

Tumor Targeting. Tumor-targeting nature of Gd(DO3A-BTA) can be visualized by adopting the literature method (Figure 1a).²³ Tumors employed for the examinations are two breast cancer cells MCF-7 and MDA-MB-231 and hepatocarcinoma SK-HEP-1, all of which exhibit strong enhancement mostly at the cytosol and the nucleus, thus demonstrating intracellular targeting nature of the present agent. It is observed for the first time that Gd(DO3A-BTA) is present both in cytosol and nucleus, although BTA itself is known to be present in both of them (vide infra for the possible mechanism of action by Gd(DO3A-BTA)). The exact amounts of gadolinium in the cytosol and the nucleus of tumor cells are provided in Table S4 (Supporting Information). Ex vivo targeting experiments provide paralleled observations for cell permeability. An almost complete overlap is made between UV-vis images of MCF-7 and that stained with a fluorophore, β -tubulin (Figure 1b). The same observations are made with MDA-MB-231 as well (Figure 1c). The degree of signal enhancement with Gd(DO3A-BTA), as expressed by contrast-to-noise ratio (CNR), is even higher and persists longer in vivo than Gd-DOTA (Figure 1d).

All in all, good correlation between the in vitro, in vivo, and ex vivo assays demonstrates intracellular tumor targeting nature of the present agent. Most notably, the formation of neither the DO3A-BTA conjugate nor Gd(DO3A-BTA) would change such tumor specificity inherent in BTA. These observations will be treated in more detail in connection with therapeutic properties of Gd(DO3A-BTA) (vide infra).

Therapy. Various BTA derivatives anchored on water-soluble moieties such as lysine and alanine are well-known for their anticancer characteristics and thus have been widely employed for imaging and therapeutic purposes.²⁴ In this regard, it would be interesting to know whether structural modification of BTA with such a chelate as DOTA and its Gd complex would render an additional entry to highly water-soluble therapeutic agents. Indeed, both DO3A-BTA conjugate

and Gd(DO3A-BTA) have revealed antitumor characteristics against three cell lines such as MCF-7, MDA-MB-231, and SK-HEP-1. All revealed apoptotic characteristics such as cell shrinkage, apoptotic bodies, and detachment from the plate on their treatment.

Morphological changes in cultured cell lines in the presence of Gd(DO3A-BTA) become apparent at the gadolinium concentration of 200 μ M and above with all cell lines. With DO3A-BTA, even higher dosage is required to observe such a change (Figure 2a). The antiproliferative activities of DO3A-BTA and Gd(DO3A-BTA) measured by CCK-8 assays render the growth suppression of the cell lines in terms of cell viability for MCF-7, MDA-MB-231, and SK-HEP-1 (Figure 2b). According to corresponding growth-inhibition 50 (GI_{50}) and total-growth-inhibition (TGI) values (Table 2), Gd(DO3A-BTA) is a little more potent than DO3A-BTA in that the former shows lower GI_{50} and TGI values for all three cell lines. When TGI values are compared among the three tumor cells, MCF-7 is the most vulnerable toward the Gd complex, and yet as far as GI_{50} is concerned, SK-HEP-1 shows the lowest value. We further investigated the effects of Gd(DO3A-BTA) on the progression of cancer cell lines through the cell cycle and on the induction of apoptotic cell death. The proportion of cells in sub-G1 phase gradually increases in all cell lines with the increase in the gadolinium concentration (Figure 2c). Here, it is to be noted that the DNA content in the sub-G1 phase amounts to the quantitative indication of the progress of apoptosis. Here the mechanism of action of DO3A-BTA or its Gd complex is the subject of further investigation, and the one suggested by others in connection with analogous benzothiazoles, i.e., compounds I (Chart 1), may be assumed to be operative as follows: selective uptake into sensitive cells followed by arylhydrocarbon receptor (AhR) binding and translocation into the nucleus, induction of the cytochrome P450 isoform (CYP) 1A1, conversion of the drug into an electrophilic reactive intermediate, and formation of extensive DNA adducts resulting in cell death.^{1,16}

The therapeutic effect of Gd(DO3A-BTA) in vivo was examined on MDA-MB-231 revealing the lowest GI_{50} of the three cell lines. Expectedly, tumor growth is suppressed on treatment with Gd(DO3A-BTA), while a sharp increase is observed on treatment with saline alone. The difference in the tumor sizes is visualized in the corresponding ex vivo images (Figure 3a), and changes in tumor volume can be measured by a caliper as well (Figure 3b). MR monitoring of the change in tumor sizes provides parallel and supportive observations for such an antiproliferative activity (Supporting Information Figure S4).

The amount of Gd accumulated in the tumor site for 24 h is 40–220 μ g Gd/g tumor (Supporting Information Figure S5 and Table S3), which falls within the range of the optimal amount (50–200 μ g Gd/g tumor) for GdNCT.¹⁶ This observation implies potentiality of Gd(DO3A-BTA) as a new and practical radiopharmaceuticals as well.

CONCLUSIONS

In conclusion, we have synthesized a bifunctional chelate DO3A-BTA and its gadolinium complex of the type [Gd-(DO3A-BTA)(H₂O)] to put into a new entry as a single theranostic agent. The kinetic inertness of the complex compares well with that of structurally related Gd-DOTA. Its R_1 relaxivity is 3.84 $mM^{-1} s^{-1}$, slightly higher than that of Gd-DOTA ($R_1 = 3.69 mM^{-1} s^{-1}$). The biodistribution pattern of in

vivo MRI compares well with those of DTPA-based, liver-specific MRI CAs such as Gd-EOB-DTPA and Gd-BOTPA in that heart and abdominal aorta are enhanced specifically and that enhancement endures as long as 1 h. The Gd complex is intracellular as well as tumor-specific, as confirmed by MR images of cytosols and nuclei of MCF-7, MDA-MB-231, and SK-HEP-1 cells. The antiproliferative activities of DO3A-BTA and its gadolinium complex Gd(DO3A-BTA) were demonstrated by GI_{50} and TGI values obtainable from the CCK-8 assays performed on the above cell lines. The Gd complex is a little more potent than the DO3A-BTA conjugate in that the former shows lower GI_{50} and TGI values for all three cell lines. When TGI values are compared among the three tumor cells, MCF-7 is the most vulnerable toward the Gd complex, and yet as far as GI_{50} is concerned, SK-HEP-1 shows the lowest value. Apoptosis of cancer cells was confirmed by the observations of the increase of the portion of cells in the sub-G1 phase in line with an increase in the Gd concentration.

■ ASSOCIATED CONTENT

Supporting Information

Relaxation rates; determination of binding constants. This material is available free of charge via the Internet at <http://pubs.acs.org>.

■ AUTHOR INFORMATION

Corresponding Authors

*For T.J.K.: phone, (+)82-53-950-5587; fax, (+)82-53-950-6594; E-mail, tjkim@knu.ac.kr.

*For Y.C.: phone, (+)82-53-420-5471; E-mail, ychang@knu.ac.kr.

Notes

The authors declare no competing financial interest.

■ ACKNOWLEDGMENTS

This work was partially supported by NRF through the Basic Science Research Program (2012-0006388 and 2011-0015353) and the Ministry of Commerce, Industry, and Energy through the Regional Technology Innovation Program (RTI01-01-01). We are most grateful to Dr. Ji-Ae Park (Molecular Imaging Research Center, Korea Institute of Radiological & Medical Science, Seoul, Korea) for her valuable assistance with the kinetic stability measurement.

■ ABBREVIATIONS USED

DO3A, 1,4,7,10-tetraazacyclododecane-1,4,7-trisacetic acid; BTA, benzothiazole aniline; GI_{50} , growth inhibition 50; TGI, total growth inhibition; BFCs, bifunctional chelates; SPECT, single photon emission computed tomography; RIT, radioimmunotherapy; MRI, magnetic resonance imaging; GdNCT, gadolinium neutron-capture; GdNPs, gadolinium nanoparticles; BNCT, boron neutron-capture therapy; TI, inversion time; CPMG, Carr–Purcell–Meiboom–Gill pulse sequence; TE, echo time; TR, repetition time; SE, spin echo; FOV, field of view; NEX, number of acquisition; ROI, regions of interest; CNR, contrast to noise ratio; DMEM, Dulbecco's Modified Eagle's Medium; RPMI, Roswell Park Memorial Institute; FBS, fetal bovine serum; HSA, human serum albumin; PBS, phosphate buffered saline; RIPA, radioimmunoprecipitation assay; CCK-8, cell counting kit-8; PFA, paraformaldehyde; PI, propidium iodide; FACS, fluorescent activated cell sorting;

CAs, contrast agents; ECF, extracellular fluid; AhR, arylhydrocarbon receptor; CYP, cytochrome P450 isoform

■ REFERENCES

- (1) Bradshaw, T. D.; Westwell, A. D. The development of the antitumour benzothiazole prodrug, Phortress, as a clinical candidate. *Curr. Med. Chem.* **2004**, *11*, 1009–1021.
- (2) Brantley, E.; Trapani, V.; Alley, M. C.; Hose, C. D.; Bradshaw, T. D.; Stevens, M. F.; Sausville, E. A.; Stinson, S. F. Fluorinated 2-(4-amino-3-methylphenyl)benzothiazoles induce CYP1A1 expression, become metabolized, and bind to macromolecules in sensitive human cancer cells. *Drug. Metab. Dispos.* **2004**, *32*, 1392–1401.
- (3) Tzanopoulou, S.; Pirmettis, I. C.; Patsis, G.; Paravatou-Petsotas, M.; Livaniou, E.; Papadopoulos, M.; Pelecanou, M. Synthesis, Characterization, and Biological Evaluation of M(I)(CO)₃(NNO) Complexes (M = Re, ^{99m}Tc) Conjugated to 2-(4-Aminophenyl)-benzothiazole as Potential Breast Cancer Radiopharmaceuticals. *J. Med. Chem.* **2006**, *49*, 5408–5410.
- (4) Tzanopoulou, S.; Sagnou, M.; Paravatou-Petsotas, M.; Gourni, E.; Loudos, G.; Xanthopoulos, S.; Lafkas, D.; Kiaris, H.; Varvarigou, A.; Pirmettis, I. C.; Papadopoulos, M.; Pelecanou, M. Evaluation of Re and (^{99m}Tc) complexes of 2-(4'-aminophenyl)benzothiazole as potential breast cancer radiopharmaceuticals. *J. Med. Chem.* **2010**, *53*, 4633–4641.
- (5) Chen, X.; Yu, P.; Zhang, L.; Liu, B. Synthesis and biological evaluation of ^{99m}Tc, Re-monoamine-monoamide conjugated to 2-(4-aminophenyl)benzothiazole as potential probes for beta-amyloid plaques in the brain. *Bioorg. Med. Chem. Lett.* **2008**, *18*, 1442–1445.
- (6) Mathis, C. A.; Wang, Y.; Holt, D. P.; Huang, G. F.; Debnath, M. L.; Klunk, W. E. Synthesis and evaluation of ¹¹C-labeled 6-substituted 2-arylbenzothiazoles as amyloid imaging agents. *J. Med. Chem.* **2003**, *46*, 2740–2754.
- (7) Martins, A. F.; Morfin, J.-F.; Kubičková, A.; Kubiček, V.; Buron, F.; Suzenet, F.; Salerno, M.; Lazar, A. N.; Duyckaerts, C.; Arlicot, N.; Guilloteau, D.; Geraldès, C. F. G. C.; Tóth, É. PiB-Conjugated, Metal-Based Imaging Probes: Multimodal Approaches for the Visualization of β -Amyloid Plaques. *J. Med. Chem. Lett.* **2013**, *4*, 436–440.
- (8) Saini, N.; Varshney, R.; Tiwari, A. K.; Kaul, A.; Allard, M.; Ishar, M. P.; Mishra, A. K. Synthesis, conjugation and relaxation studies of gadolinium(III)-4-benzothiazol-2-yl-phenylamine as a potential brain specific MR contrast agent. *Dalton Trans.* **2013**, *42*, 4994–5003.
- (9) Katz, E.; Willner, I. Integrated nanoparticle-biomolecule hybrid systems: synthesis, properties, and applications. *Angew. Chem., Int. Ed. Engl.* **2004**, *43*, 6042–6108.
- (10) Chen, K.; Li, Z. B.; Wang, H.; Cai, W.; Chen, X. Dual-modality optical and positron emission tomography imaging of vascular endothelial growth factor receptor on tumor vasculature using quantum dots. *Eur. J. Nucl. Med. Mol. Imaging* **2008**, *35*, 2235–2244.
- (11) Steiniger, S. C.; Kreuter, J.; Khalansky, A. S.; Skidan, I. N.; Bobruskin, A. I.; Smimova, Z. S.; Severin, S. E.; Uhi, R.; Kock, M.; Geiger, K. D.; Gelperina, S. E. Chemotherapy of glioblastoma in rats using doxorubicin-loaded nanoparticles. *Int. J. Cancer* **2004**, *5*, 759–767.
- (12) Akine, Y.; Tokita, N.; Tokuyue, K.; Satoh, M.; Fukumori, Y.; Tokumitsu, H.; Kanamori, R.; Kobayashi, T.; Kanda, K. Neutron-Capture Therapy of Murine Ascites Tumor with Gadolinium-Containing Microcapsules. *J. Cancer Res. Clin. Oncol.* **1992**, *119*, 71–73.
- (13) De Jong, W. H.; Borm, P. J. Drug delivery and nanoparticles: applications and hazards. *Int. J. Nanomed.* **2008**, *3*, 133–149.
- (14) William, W. N., Jr.; Zinner, R. G.; Karp, D. D.; Oh, Y. W.; Glisson, B. S.; Phan, S. C.; Stewart, D. J. Phase I trial of motexafin gadolinium in combination with docetaxel and cisplatin for the treatment of non-small cell lung cancer. *J. Thorac. Oncol.* **2007**, *2*, 745–750.
- (15) Crossley, E. L.; Aitken, J. B.; Vogt, S.; Harris, H. H.; Rendina, L. M. Selective aggregation of a platinum–gadolinium complex within a tumor-cell nucleus. *Angew. Chem., Int. Ed. Engl.* **2010**, *49*, 1231–3.

(16) Shih, J. L. A.; Brugger, R. M. Gadolinium as a Neutron-Capture Therapy Agent. *Med. Phys.* **1992**, *19*, 733–744.

(17) Salt, C.; Lennox, A. J.; Takagaki, M.; Maguire, J. A.; Hosmane, N. S. Boron and gadolinium neutron capture therapy. *Russ. Chem. Bull. Int. Ed.* **2004**, *53*, 1871–1888.

(18) Crossley, E. L.; Ziolkowski, E. J.; Coderre, J. A.; Rendina, L. M. Boronated DNA-binding compounds as potential agents for boron neutron capture therapy. *Mini-Rev. Med. Chem.* **2007**, *7*, 303–313.

(19) Yamamoto, T.; Nakai, K.; Matsumura, A. Boron neutron capture therapy for glioblastoma. *Cancer Lett.* **2008**, *262*, 143–152.

(20) Laurent, S.; Elst, L. V.; Copoix, F.; Muller, R. N. Stability of MRI paramagnetic contrast media—a proton relaxometric protocol for transmetalation assessment. *Invest. Radiol.* **2001**, *36*, 115–122.

(21) Avedano, S.; Tei, L.; Lombardi, A.; Giovenzana, G. B.; Aime, S.; Longo, D.; Botta, M. Maximizing the relaxivity of HSA-bound gadolinium complexes by simultaneous optimization of rotation and water exchange. *Chem. Commun.* **2007**, 4726–4728.

(22) Henrotte, V.; Vander Elst, L.; Laurent, S.; Muller, R. N. Comprehensive investigation of the non-covalent binding of MRI contrast agents with human serum albumin. *J. Biol. Inorg. Chem.* **2007**, *12*, 929–937.

(23) Yamane, T.; Hanaoka, K.; Muramatsu, Y.; Tamura, K.; Adachi, Y.; Miyashita, Y.; Hirata, Y.; Nagano, T. Method for enhancing cell penetration of Gd³⁺-based MRI contrast agents by conjugation with hydrophobic fluorescent dyes. *Bioconjugate Chem.* **2011**, *22*, 2227–2236.

(24) Ian Hutchinson, S. A. J.; Vishnuvajjala, B. R.; Westwell, A. D.; Stevens, M. F. G.; Westwell, A. D. Antitumor Benzothiazoles. 16.1. Synthesis and Pharmaceutical Properties of Antitumor 2-(4-Aminophenyl)benzothiazole Amino Acid Prodrugs. *J. Med. Chem.* **2002**, *45*, 744–747.

(25) Gu, S.-W.; Kim, H.-K.; Kang, B.-S.; Chang, Y.; Kim, T.-J. Gd-Complexes of 1,4,7,10-tetraazacyclododecane-*N,N',N'',N'''*-1,4,7,10-tetraacetic acid (DOTA) conjugates of tranexamates as a new class of blood-pool magnetic resonance imaging contrast agents. *J. Med. Chem.* **2011**, *54*, 143–152.

(26) Lokling, K. E.; Fossheim, S. L.; Klaveness, J.; Skurtveit, R. Biodistribution of pH-responsive liposomes for MRI and a novel approach to improve the pH-responsiveness. *J. Controlled Release* **2004**, *98*, 87–95.

(27) Kubota, T.; Kubouchi, K.; Koh, J.; Enomoto, K.; Ishibiki, K.; Abe, O. Human Breast Carcinoma (MCF-7) Serially Transplanted into Nude Mice. *Jpn. J. Surg.* **1983**, *13*, 381–384.